

## Performance Evaluation of Composite Electrolyte with GQD for All-Solid-State Lithium Batteries

Sung Won Hwang and Dae-Ki Hong\*

Department of System Semiconductor Engineering, SangMyung University, Cheonan-si, 31066, Korea

\*Corresponding Author: Dae-Ki Hong. Email: hongdk@smu.ac.kr

Received: 19 February 2022; Accepted: 06 May 2022

**Abstract:** The use of a stabilized lithium structure as cathode material for batteries could be a fundamental alternative in the development of next-generation energy storage devices. However, the lithium structure severely limits battery life due to safety concerns caused by the growth of lithium (Li) dendrites during rapid charge/discharge cycles. Solid electrolytes, which are used in high-density energy storage devices and avoid the instability of liquid electrolytes, can be a promising alternative for next-generation batteries. Nevertheless, poor lithium ion conductivity and structural defects at room temperature have been pointed out as limitations. In this study, through the application of a low-dimensional graphene quantum dot (GQD) layer structure, stable operation characteristics were demonstrated based on  $\text{Li}^+$  ion conductivity and excellent electrochemical performance. Moreover, the device based on the modified graphene quantum dots (GQDs) in solid state exhibited retention properties of 95.3% for 100 cycles at 0.5 C and room temperature (RT). Transmission electron microscopy analysis was performed to elucidate the  $\text{Li}^+$  ion action mechanism in the modified GQD/electrolyte heterostructure. The low-dimensional structure of the GQD-based solid electrolyte has provided an important strategy for stably-scalable solid-state lithium battery applications at room temperature. It was demonstrated that lithiated graphene quantum dots (Li-GQDs) inhibit the growth of Li dendrites by regulating the modified  $\text{Li}^+$  ion flux during charge/discharge cycling at current densities of 2.2–5.5 mA cm<sup>2</sup>, acting as a modified Li diffusion heterointerface. A full Li GQD-based device was fabricated to demonstrate the practicality of the modified Li structure using the Li–GQD hetero-interface. This study indicates that the low-dimensional carbon structure in Li–GQDs can be an effective approach for stabilization of solid-state Li matrix architecture.

**Keywords:** Solid-state; lithium batteries; composite electrolyte; quantum dot; graphene



This work is licensed under a Creative Commons Attribution 4.0 International License, which permits unrestricted use, distribution, and reproduction in any medium, provided the original work is properly cited.

## 1 Introduction

Recently, the demand for high-performance batteries has exploded, and all-solid-state lithium metal batteries are receiving great attention to satisfy the demand for high density energy systems. All-solid-state lithium batteries are replacing liquid electrolytes. Because there is no risk of battery explosion, and because high energy density is possible, such solid-state batteries represent a new generation of battery technology [1–3]. The capacity of a battery is determined by the quantity of  $\text{Li}^+$  ions that move, and the  $\text{Li}^+$  ion conductivity of the electrolyte affects the charging and discharging rates of the battery [4–6]. To achieve high energy density, it is important to develop a battery with high voltage and large capacity; for high output, it is necessary to increase the quantity of  $\text{Li}^+$  ions and electrons that move [7–10]. Conventional rechargeable lithium-ion batteries have revolutionized powertrains for electric vehicles. Additional innovations include small energy storage devices and eco-friendly wearable devices. However, with the move toward usage of solid materials, the current level of lithium-ion battery structure has limitations in energy storage capacity and stability.

A modified metal electrode in which the lithium (Li) to host material ratio is extended is capable of more than doubling the theoretical energy density at the heterogeneous interface. Among anode materials, Li metal has high theoretical specific capacity and low electrochemical potential. Nevertheless, the heterogeneous reaction properties at the heterogeneous interface lead to the spontaneous formation of inhomogeneous and brittle solid electrolyte interfaces (SEIs), also known as dendrites, and electrical short-circuit reactions upon rupture [11–14]. This issue not only poses a safety risk due to side reactions caused by Li dendrites, but also creates a vicious cycle of low coulombic efficiency and shortened lifespan. Existing studies on Li metal stabilization have suggested using additives to improve  $\text{Li}^+$  ion transport and control the metal surface, or the development of solid electrolytes that can act as physical barriers to dendrite propagation [15–20].

Here, we use a low-dimensional quantum dot structure to control the  $\text{Li}^+$  ion flux and Li deposition; this structure suppresses dendrite formation and forms Li diffusion interfaces based on lithiated graphene quantum dots (Li-GQDs). The use of graphite and carbon nanotubes for Li dendrite suppression has been explored, but less attention has been paid to the role that a modified interface between Li and carbon can contribute to battery structure stabilization. A positively charged, low-dimensional GQD matrix structure was obtained through a chemical exfoliation process; this structure has fewer defects than the bulk structure and the active site are reactive. Here, by exploring the heterojunction between Li and GQDs, in-depth study of the Li–carbon hetero-structure was conducted to promote dendrite inhibition. The spontaneous reaction of Li metal and the dissimilar materials when no electric potential is applied indicates the potential for passivation of the Li anode. Li can form an alloy upon contact with a non-metal or intercalated  $\text{Li}^+$  ions, maintaining charge properties and reducing stacking defects. Because it is only activated at high potentials, the carbon structure as a hetero-interfacial layer enables selective conversion of  $\text{Li}^+$  ions by preventing reaction of the layer with larger anions [21–24].

In this work, we formed a passivation structure for the Li anode metal layer using GQD-based  $\text{Li}^+$  ion control. Because the contact between particles is not smooth due to pores between the defects present inside the electrode and the solid electrolyte, the effective contact area through which lithium ions move is low, making it difficult to realize high battery performance. However, this new technology designed using a low-dimensional structure maximizes the effective contact area between cathode material and solid electrolyte so that lithium ions can move smoothly; a low-defect GQD layer is formed. By using a solid electrolyte coated with GQD layer to fill in defects and pores inside the electrode during device fabrication, the interfacial resistance during lithium ion movement was

effectively improved [25–27]. We have demonstrated a heterointerface design that incorporates a low-dimensional GQD layer into a heterostructure matrix to provide robust interfacial stabilization. The Li metal structure is shown in Fig. 1b, in which it can be seen that the GQD layer with high mass density was wetted with a highly concentrated electrolyte. Li dendrite growth was effectively suppressed due to the  $\text{Li}^+$  flux of the modified Li metal interface and the excellent mechanical strength of the homogeneous GQD layer.

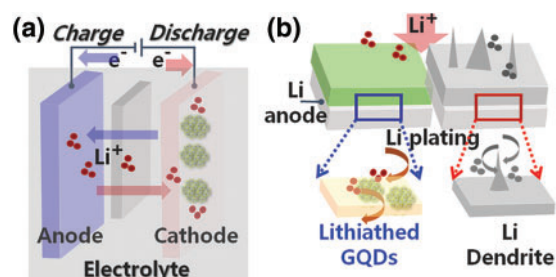


**Figure 1:** Schematic of Lithium (Li)-Ion battery mechanism, lithium dendrite in all-solid-state batteries: growth mechanisms

Physical contact between Li and GQD layers resulted in spontaneous reduction of the modified GQD layers, which was balanced by the control of  $\text{Li}^+$  ions. It was hypothesized that the Li-GQD hetero-interface acts as a mediator to control Li diffusion and prevent the growth of dendrites. During battery charging,  $\text{Li}^+$  ions of the Li-GQD layer were deposited on the Li metal surface and then replaced with  $\text{Li}^+$  ions of the electrolyte. The reduction change of the GQD layer was confirmed only in the region in close contact with the Li metal; spontaneous lithiation proceeded due to the generation of an electrochemical potential at the heterogeneous interface and the Fermi level difference. The heterostructure of the Li-GQD layer did not change under potential-induced lithiation, and no bulk deposits or leakage defects were observed, indicating the formation of uniform SEI-layer Li-GQD thin film. To our knowledge, this is the first report of a low-dimensional GQD-based all-solid-state battery operating stably at room temperature.

## 2 Experiment

### 2.1 Preparation of Graphene Quantum Dots (GQDs)

Graphene was synthesized on Cu foil in a thermal furnace at 950°C for 7 min under Argon (Ar): Hydrogen 2 ( $\text{H}_2$ ): methane ( $\text{CH}_4$ ) mixed-gas flow. Subsequently, a pre-prepared poly (methyl methacrylate) (PMMA, Sigma Aldrich) solution was dropped all over the graphene surface, spin-coated at 5000 rpm for 45 s, and then heat treated on a hot plate at 160°C for 3 min. The PMMA solution was prepared by adding 0.5 g PMMA powder to 15 mL chlorobenzene (Sigma Aldrich) and stirring the mixture at 65°C for 8 h. The Cu was removed by dipping the PMMA/graphene/Cu foil stack in 1 mole (M) Iron (III) chloride ( $\text{FeCl}_3$ ) solution (Sigma Aldrich). The PMMA/graphene stack was then transferred onto glass or polyethylene terephthalate (PET) substrate and heat-treated at 110°C for 3 h. Finally, the PMMA was dissolved by acetone. The following processes were used to fabricate GQDs. Graphene oxide (GO) was prepared from graphite powder using the Hummers method. GO was deoxidized in a horizontal furnace at 350°C–450°C for four hours under Ar to produce reduced graphene oxide powder. About 5.0–6.5 g of graphene oxide powder was oxidized by ultrasonication in concentrated 15 mL sulfuric acid ( $\text{H}_2\text{SO}_4$ ) and 40 mL nitric acid ( $\text{HNO}_3$ ) for 20 h. In addition, 350 mL deionized water was used to dilute the mixture. After cooling to room temperature, the

resulting powder was redispersed in 35-mL DI water for two hours under ultrasonication. Then, by filtering the resulting suspension through a 200 nanometer (nm) nano-porous membrane, a brown solution was separated. Since the colloidal solution still contained some large graphene nanoparticles (<200 nm) emitting weak blue fluorescence, it was further filtered overnight in a dialysis bag with a cutoff of 3500 dalton (Da) molecular weight, thereby producing strongly fluorescent GQDs. The GQDs were separated into different sizes using several dialysis bags of 1000–50,000 Da and a 20-nm nano-porous membrane.

## 2.2 Cell Fabrication

To fabricate solid-state Li batteries (SSLBs)-based nano-structure devices, after the direct synthesis of the extracted graphene, graphene quantum dots (GQDs) of each shape were directly grown on patterned Li electrodes on a copper (Cu) thin films through a modified chemical vapour deposition (CVD) method. After washing the composite GQD layer in a deionized water cleaning process, heat treatment was performed. Coin cells were assembled in glove box using CR2032 type shells. The modified PEO electrolyte membrane was prepared by drying a mixture of polyethylene oxide (PEO), Lithium bis(trifluoromethanesulphonyl) imide (LiTFSI) powders, and acetonitrile in a vacuum oven at 50°C for 24 h [28–30]. The symmetrical cells with GQD-PEO-LiTFSI hybrid paste were fabricated with two Li disks (thickness of 200  $\mu\text{m}$ ) and a donut spacer (thickness of 25  $\mu\text{m}$ ). GQD-PEO-LiTFSI hybrid paste was placed in the middle of spacer. The interlayer was built with 10  $\mu\text{L}$  commercial LE (1 m  $\text{LiPF}_6$  in ethylene carbonate/diethyl carbonate mixture solvent) or 15 mg paste hybrid on each side of pellet. The interlayer in full cells was built in the same way for symmetric cells [31–33].

## 2.3 Characterization

Plane- and cross-sectional-view images of the materials and devices were obtained by field emission scanning electron microscopy (FE-SEM, Carl Zeiss, model LEO SUPRA 55). Morphologies of GQDs were analyzed using an High-resolution Transmission Microscopy (HRTEM) (FEI Tecnai F30 S-Twin). To make the HRTEM specimens, the GQDs were dispersed in DI water, drops of which were then put on C- or SiO-coated Cu grids (Tedpella, Inc., Redding, CA, USA) and mica substrate, respectively. The current-voltage (I–V) curve of the device was analyzed using an electrical and electronic workstation (Keithley 2400). Current density-voltage (J–V) characteristics were monitored by forward/reverse scans at 200 ms and 10 mV under standard conditions. The ionic conductivity of the electrolytes was measured on a dielectric spectrometer in the temperature range from  $-20^\circ\text{C}$  to  $100^\circ\text{C}$  in a gold-plated cell with Teflon spacer. Lithium samples were transferred from glovebox to the chamber in a vessel without explosion in air. Raman spectra were observed from a Bruker IFS66 Fourier Transform spectrometer with a FRA106 Raman module. All the heating tests were carried out in Ar-filled glove box. Electrochemical impedance spectroscopy was performed on a Reference 600 (Gamry Instruments) over a frequency range of 0.01 to 1 MHz and the perturbation amplitude was 10 mV.

## 3 Results and Discussion

### 3.1 Li-Ion Battery Mechanism and Lithium Dendrite in Solid-State Batteries

As shown in Fig. 1, a lithium secondary battery consists of a positive electrode, an electrolyte, and a gold electrode, a polymer separator with thickness of tens to hundreds of micrometers is positioned inside a liquid electrolyte comprising organic solvent and lithium salt. Movements of lithium ions are in opposite directions during charging and discharging. In other words, during discharge,  $\text{Li}^+$

ions move from the negative to the positive electrode, and electrons generated as lithium ionizes also transfer in the same direction. The cause of this  $\text{Li}^+$  ion migration is the system's pursuit of chemical stability against the potential difference between the two electrodes. Li dendrite growth, which unexpectedly penetrates the separator during charge/discharge operation and causes battery failure and fire, has severely limited the use of next-generation devices as well as various high-performance system applications. Therefore, next-generation batteries require a transition from the existing layered structure to a modified electrode structure that can control the intercalation of lithium between graphite layers.

The electrical properties of the sample according to the  $\text{I}_2$  content of the modified poly (ethylene oxide) (PEO) structure are shown in Fig. 2a. For ionic modulation of the PEO structure, the ionic conductivities of electrolytes with different GQD- $\text{I}_2$  contents (1, 1.5 and 2 wt% of PEO-LiTFSI) were measured. It was found that the ionic conductivity of the sample structures depends on the temperature [34]. Compared with pristine PEO-LiTFSI, when 1.5 wt%  $\text{I}_2$  was added to the PEO-LiTFSI electrolyte at  $50^\circ\text{C}$ , the resulting electrolyte saw its ionic conductivity increase from  $9.34 \times 10^{-6}$  to  $6.28 \times 10^{-5}$   $\text{S cm}^{-1}$ . The ionic conductivity tends to increase with increasing temperature of the modified PEO-GQD based electrolyte.

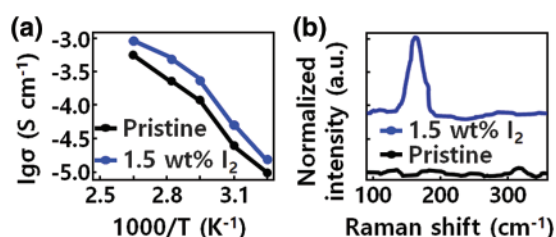


**Figure 2:** (a) Ionic conductivities of the GQD-PEO-based electrolyte with Iodine ( $\text{I}_2$ ) contents. (b) Raman spectra of pristine PEO and GQD-modified PEO- Lithium bis(trifluoromethanesulphonyl) imide (LiTFSI)-1.5 weight (wt) %

In Fig. 2b, Raman spectroscopy was performed to investigate the effect of  $\text{I}_2$  on the ionic conductivity. The characteristic band at  $190 \text{ cm}^{-1}$  belongs to  $\text{I}_2$ , but this characteristic peak was not observed in the GQD-modified PEO-LiTFSI-1 wt %  $\text{I}_2$  sample. In contrast, in the GQD-modified PEO-LiTFSI-1.5 wt %  $\text{I}_2$  sample, a significant band between  $130$  and  $200 \text{ cm}^{-1}$  was observed due to the activation of symmetric stretching mode of the  $\text{I}_3^-$ -atomic structural unit. This indicates that iodine exists in  $\text{I}_3^-$  rather than  $\text{I}_2$  form in the GQD-modified PEO polymer structure. Through spectroscopic analysis of  $\text{I}_2$  dissolved in acetonitrile, the properties of  $\text{I}_3^-$  were confirmed. Unlike the  $145 \text{ cm}^{-1}$  peak, related to  $\text{I}_3^-$ , the characteristic  $190 \text{ cm}^{-1}$  peak of  $\text{I}_2$  was dominant. According to this result,  $\text{I}_3^-$  is mainly generated by interaction between  $\text{I}_2$  and PEO, in a reaction controlled by GQD.

When  $\text{I}_2$  was dissolved in acetonitrile, it received electrons from the modified PEO, an electron donating structure, and generated  $\text{I}^-$  through a reduction reaction. As a result,  $\text{I}^-$  ions generated  $\text{I}_3^-$ , an anion, through a chemical reaction with  $\text{I}_2$ . The interaction between PEO and  $\text{I}_2$ , as well as the donor-acceptor relationship between iodine species and acceptor, is widely known through the results of previous studies on organic molecular phenomena in water-insoluble solvents. The chemical movement of hydrogen atoms according to different amounts of  $\text{I}_2$  in the modified PEO structure (PEO-x wt %  $\text{I}_2$ ,  $x = 2, 4, 6$ ) is smaller than that in the original PEO structure, and results show that chemical movement increases as the density of  $\text{I}_2$  increases. This indicates the complex action at the interface produced by GQDs between  $\text{I}_3^-$ -units and PEO molecules.

As a result, the  $I_2$  surface structure modified by GQD reduces the crystallinity of PEO and promotes electron transfer in the PEO hetero-interface structure. GQD-modified  $I_3^-$  interacts with the carbon-oxygen of the electron-donating substitutes to effectively weaken the bonding force between  $Li^+$  ions and other oxygen groups, promoting efficient transport of  $Li^+$ . As a result, this process contributes to the enhancement of the ionic conductivity of the GQD-modified electrolyte. Compared with that of the pristine PEO structure, the diffraction intensity of modified PEO-LiTFSI decreased, indicating that there was a change in crystallinity. It was confirmed that  $I_2$  doping can significantly reduce the effective contact resistance of the modified GQD-PEO, and can control the crystallinity through the action of GQD. In addition, GQD-based  $I_2$  doping does not affect the electrochemical behavior of the composite electrolyte. We investigate the electrochemical properties of various hetero-interfaces used to stabilize Li metal anodes of Li batteries with symmetric structure. All devices are rated at a fixed capacity of  $0.2 \text{ mAh cm}^{-2}$  and a current density of  $0.2 \text{ mA cm}^{-2}$ .

### 3.2 Solid-State Lithium Batteries based on Nanocomposite Electrolyte with GQD

Fig. 3 shows the cell using pristine PEO-LiTFSI electrolyte had an average overpotential of 120 mV and exhibited a limited cycle life of 385 h. Further analysis of the micro-surface morphology of the Li layer by scanning electron microscopy (SEM) revealed that a sharp drop in overpotential occurred during repeated charge/discharge cycles, indicating a short circuit. A porous Li metal surface can be observed in Fig. 3d. The void defects inhibit  $Li^+$  ion diffusion and accelerate formation of Li dendrites in the hetero-interface structure [35]. As a result, device performance such as lifetime and durability deteriorated. In contrast, devices using GQD-modified PEO-LiTFSI- $x \text{ wt}\% I_2$  ( $x = 1$  and 1.5) electrolytes had improved cycling stability. Through the interfacial Li plating and stripping process, dense structural defects were improved at the interface between the GQD-modified PEO-LiTFSI-1.5 wt%  $I_2$  electrolyte and Li metal.

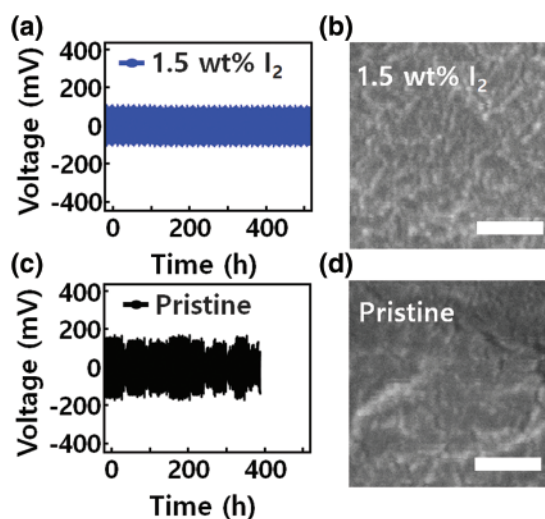


**Figure 3:** (a and c) Voltage profiles of symmetric cells with different electrolytes interlayer operated at a current density of  $0.1 \text{ mA cm}^{-2}$  and  $45^\circ\text{C}$ . (b and d) Morphology of cycled Li metal anodes. Top view SEM images of cycled Li anode using pristine and GQD-PEO-LiTFSI-1.5 wt%  $I_2$  electrolyte in low-magnification. Scale bar, 500 nm

In particular, the GQD-modified PEO-LiTFSI-1.5 wt % I<sub>2</sub> electrolyte had a long lifetime of more than 550 h and a rather low average overpotential of 55 mV, leading to negligible polarization. The Li metal anode showed a generally uniform surface and stable cycling performance without serious defects on the surface or at the interface. The GQD-modified PEO-LiTFSI-1.5 wt% I<sub>2</sub> electrolyte presents a low polarization of 0.2 mA cm<sup>-2</sup>. Moreover, the battery performance of devices composed of electrolytes containing 1.5 wt % I<sub>2</sub> ions was superior to those containing I<sub>2</sub> ions at percentages of 0.5, 1.0, and 3 wt %. However, I<sub>3</sub><sup>-</sup> reacted chemically with the unstable Li structure, composed disproportionately of Li interfaces and GQD-Li<sub>2</sub>O. The unstable structure of the I<sub>3</sub><sup>-</sup> ion caused corrosion of the active Li structure, indicating contact issues between Li layer and GQD and poor battery performance.

Likewise, a moderate reaction of GQD-modified iodine to reduce overpotential is confirmed with different current densities. This indicates a significant enhancement effect of GQD-modified I<sub>2</sub>-ion on the interfacial stability between the GQD-electrolyte and the Li layer.

To confirm the mechanism of GQD-modified I<sub>2</sub> doping on the surface and interfacial stability, observed the morphology and composition of the interface at atomic scale by measuring (transmission electron microscopy) TEM. The low-magnification TEM image in Fig. 4a shows the interface observed without I<sub>2</sub> doping. In the high-resolution-TEM (HR-TEM) images of the blue and yellow square region in Fig. 4b, crystalline Li layer and GQD-Li<sub>2</sub>O regions are visible. In addition, the high oxygen content and oxygen atoms at the interface between the pristine PEO-LiTFSI electrolyte and the Li anode formed a Lithium oxide (Li<sub>2</sub>O) structure [36]. Compared with the case without I<sub>2</sub> doping, it did not change the defect structure at the interface. In the HR-TEM images in Figs. 4c and 4d, Li<sub>2</sub>O and GQD nanocrystal regions and an amorphous layer can be seen to be mixed, and an I-doped organic-inorganic layer can be observed.

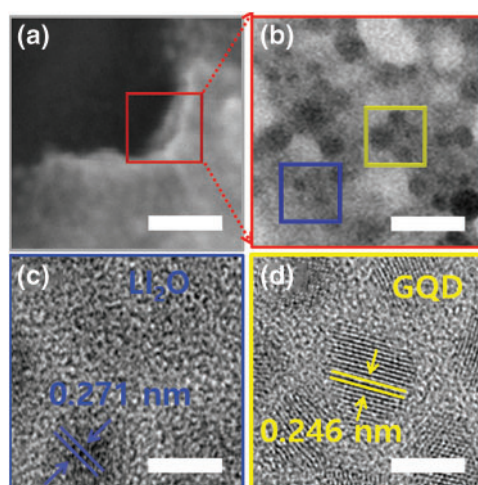


**Figure 4:** (a and b) TEM images of the distribution of the SEI components with GQD-PEO-LiTFSI-1.5 wt % I<sub>2</sub> electrolyte. Scale bar, 500 nm, 20 nm, respectively. (c and d) corresponding high-resolution transmission electron microscopy (HR-TEM) images obtained in the blue and yellow rectangular region of (b), respectively. Scale bar, 2 nm

Crystal structures and grid spacing corresponding to Li, Li<sub>2</sub>O, Lithium iodide (LiI), and Lithium iodide oxide (LiIO<sub>3</sub>) were can be observed in Figs. 4c and 4d. An Li layer with lattice spacing of 2.48 Å. The lattice spacings of 2.71 and 2.46 Å corresponded to the Li<sub>2</sub>O (111) and GQD planes. The

LiI layer distributed on the surface of the  $\text{Li}_2\text{O}$  structure and  $\text{Li}_2\text{O}$  domains has been recognized as a solid polymer electrolytes (SPEs) interfacial reactant with Li. The LiI structure forms due to the rapid reaction between  $\text{I}_3^-$  and Li/GQD- $\text{Li}_2\text{O}$ . In addition, the formation of  $\text{LiIO}_3$  took place via different interfacial reactions according to the  $\text{I}_3^-$ -doping and  $\text{Li}_2\text{O}$  content. This can be confirmed by the contents of the various nanostructure at the interface after Li formation. The TEM results indicate that GQD-based  $\text{I}_2$  doping can achieve uniform formation of Li layer by construction of modified SEI interfacial layer (LiI/GQD- $\text{LiIO}_3$ ). Controlled  $\text{I}_3^-$  reacts with Li and  $\text{Li}_2\text{O}$  at the interface to generate activated  $\text{Li}^+$  ions and this leads to a defect-free stable interface, which can enhance  $\text{Li}^+$  ion conduction at the heterostructure.

The solid-state batteries with GQD-PEO-LiTFSI-1.5 wt%  $\text{I}_2$  electrolyte also indicate a good rate capability, as shown in Fig. 5a, High capacities of 152, 148, and 146  $\text{mAh g}^{-1}$  are delivered at, respectively, 50, 100, and 200  $\mu\text{A cm}^{-2}$ . The capacity recovers to 149  $\text{mAh g}^{-1}$  when the current returns to 100  $\mu\text{A cm}^{-2}$ . Further evaluation of the electrochemical stability of the GQD-PEO layer was conducted with a cycling test in an GQD-PEO-LiTFSI-1.5 wt% Li cell at 150  $\mu\text{A cm}^{-2}$ , a stabilized capacity of 149  $\text{mAh g}^{-1}$  is delivered after an activation reaction in the first several cycles.

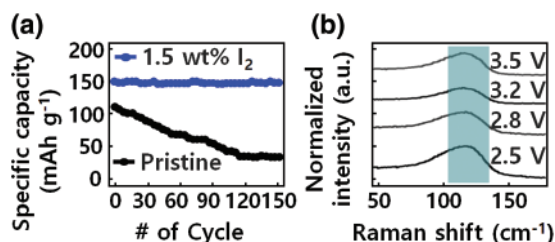


**Figure 5:** Electrochemical performance of solid-state batteries with GQD-PEO-LiTFSI-1.5 wt%  $\text{I}_2$  electrolyte. (a) cycling stability, and (b) Raman characterization of the interphase between GQD-PEO electrolyte and Li metal

In Fig. 5b, Raman spectra results show the composition of the modified atomic layer interface and the chemical reaction of the iodine species. The components of the intermediate phase appearing in the PEO-based device structure are  $\text{Li}_2\text{O}$  and an amorphous composite polymer; this intermediate phase becomes a large source of resistance to ion conduction. With GQD-modified  $\text{I}_2$  doping, there was no significant change in oxygen content at the heterostructure interface, and the oxygen content of  $\text{Li}_2\text{O}$ , compared to that of  $\text{Li}_{6.4}\text{La}_3\text{Zr}_{1.4}\text{Ta}_{0.6}\text{O}_{12}$ , decreased. As a result, the composition of the GQD-based I-doped hetero-interface, which can control defects between the GQD-modified electrolyte and Li structure.

The properties of elemental iodine on the electrolyte interface before and after the repeated operation indicated that the structure of  $\text{I}_2$  deteriorated and the amount of I- component increased, indicating that the  $\text{LiI}_3$  moiety was reduced to an LiI layer by Li atoms [37]. The change of the  $\text{I}_3^-$  structure in the modified GQD-PEO-LiTFSI-1.5 wt% I electrolyte was measured by Raman spectra analysis during charge/discharge cycles of transparent  $\text{LiFePO}_4/\text{PEO-LiTFSI-1 wt% I}_2$  GQD/Li devices. A pathway to stabilize Li was realized by spontaneous formation of a modified LiI layer between the composite polymer/GQD/Li hetero-interface. In the signal range of 0 to 200  $\text{cm}^{-1}$ , a peak appeared at 128  $\text{cm}^{-1}$ , which corresponds to the symmetric stretching mode of the  $\text{I}_3^-$  structure. The peak at 128  $\text{cm}^{-1}$  decreases during the charge/discharge cycle, indicating that modified  $\text{I}_3^-$  reacts with Li and  $\text{Li}_2\text{O}$  to form a hetero-interfacial passivation layer of LiI and  $\text{LiIO}_3$ . The reduction of modified  $\text{I}_3^-$  by Li and  $\text{Li}_2\text{O}$  can be described by the  $\text{Li}^+$  and  $\text{IO}_3^-$ -ion reactions.

To design a hetero-interface with improved structural reliability between the Li metal anode and the GQD-modified PEO-LiTFSI-1.5 wt% I<sub>2</sub> electrolyte, a modified transparent LiFePO<sub>4</sub> anode, Li metal anode, and electrolyte were fabricated at 50°C and evaluated via SSLB. The LiFePO<sub>4</sub>/Li device to which the pristine PEO-LiTFSI electrolyte was applied showed rapid capacity deterioration, with a capacity retention rate of 43.6% after 100 cycles. In contrast, by applying the GQD-modified electrolyte, the LiFePO<sub>4</sub>/Li device showed moderate capacity retention and stable movement at 0.5 C, as can be seen in Fig. 6a. After 100 cycles, the GQD-modified device provides a specific capacity of 148 mAh g<sup>-1</sup> and a capacity retention of 94.8%. Moreover, batteries using modified electrolytes with GQDs have capacities higher than those of pristine devices. As a result, the GQD-controlled iodine matrix significantly increased the effective area of Li<sup>+</sup> ion transport because the hetero-interface and electrolyte inside contribute to battery capacity enhancement [38].

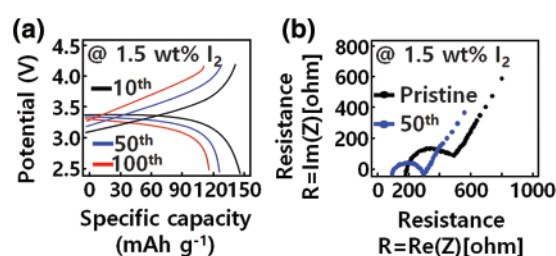


**Figure 6:** Electrochemical performances of solid-state Li battery. (a) Charge curves of GQD-PEO-LiTFSI-1.5 wt% I<sub>2</sub>/Li cells. (b) Impedance spectrum at various electrolytes before and after 50 cycles

The pristine electrolyte and the GQD-based I-doped electrolyte showed typical charge/discharge characteristics of transparent LiFePO<sub>4</sub> devices, as shown in Fig. 6a. In addition to the voltage of 3.25 and 3.40 V corresponding to LiFePO<sub>4</sub>, SSLB containing GQD-PEO-LiTFSI-1.5 wt % I<sub>2</sub> electrolyte modified with GQD also has a 3.14 V discharge characteristic, caused by the state change of modified I<sub>3</sub><sup>-</sup>. This is consistent with the nanostructure properties. The control made possible by use of 1.5 wt % I<sub>2</sub> modified with GQDs revealed the reversible redox properties of LiFePO<sub>4</sub>, indicating a reduction of I<sub>3</sub><sup>-</sup> to I<sup>-</sup> and oxidation of I<sup>-</sup> to I<sub>3</sub><sup>-</sup> due to GQD. This suggests that the GQD-modified iodine structure is involved in the electrochemical change of the device. In addition, the SSLB using the modified GQD-PEO-LiTFSI-1.5 wt % I<sub>2</sub> electrolyte showed superior rate characteristics compared to those of the pristine electrolyte.

Subsequently, using EIS measurement, changes of SSLB interface impedance ( $R_{ct}$ ) after repeated cycles were analyzed to determine the hetero-interfacial structural stability between the GQD-modified PEO electrolyte and the Li interface. As shown in Fig. 6b,  $R_{ct}$  showed a tendency to increase after continuously changing cycle of the SSLB containing modified PEO-LiTFSI electrolyte. And, the  $R_{ct}$  of the device using the modified GQD-PEO-LiTFSI-1.5 wt % I<sub>2</sub> electrolyte was smaller than that of the device using the pristine PEO-LiTFSI electrolyte. After 10, 50, and 100 cycles, the  $R_{ct}$ s of the devices were 254, 102, and 86  $\Omega$ , respectively. These results indicate that GQD-based modified I<sub>2</sub> doping is responsible for the structuring of the highly conductive modified SEI layer with GQDs, and is related to the formation of the Li/Li<sub>2</sub>O structure by iodine redox reaction. The hetero-interface impedance between Li anode and GQD-PEO electrolyte decreased.

## 4 Conclusion

A modified structure of  $I_2$  was applied to a GQD-PEO-based hetero-structured electrolyte. During the SPEs structuring process, iodine underwent  $I_2$  to  $I_3^-$  conversion and reacted with the carbon–oxygen bond of the modified PEO, improving the ionic conductivity of the hetero-composite electrolyte by a factor of 5. In addition, changes of position of I-doped LiI and the  $LiIO_3$  structure at the Li metal anode interface are attributed to the stable diffusion of iodine in the GQD-modified electrolyte. An SEI layer comprised of iodide and  $Li_2O$  hetero-interfaces in the amorphous Li structure was formed, inhibiting the growth of Li dendrites through a reaction between GQD-modified electrolyte and Li metal anode. In addition, GQD-modified  $I_3^-$  reacts with Li and  $Li_2O$  structures allowing control of the Li metal anode hetero-interface. Due to the effect of GQD-modified  $I_2$  doping, the GQD/PEO LiTFSI-1.5 wt %  $I_2$ /Li device exhibited stable rate capacity and good cycling performance. These aspects of heterostructure control and electrolyte design based on halogen-related reactions suggest an effective strategy for an optimal SSLBs system, and can be used to design low-dimensional structure-based halide applications for complex electrolytes.

**Funding Statement:** This research was funded by a 2020 research Grant from Sangmyung University.

**Conflicts of Interest:** The authors declare that they have no conflicts of interest to report regarding the present study.

## References

- [1] J. Janek and W. G. Zeier, “A solid future for battery development,” *Nature Energy*, vol. 1, no. 16141, pp. 1–4, 2016.
- [2] S. Gupta, “From gadgets to the smart grid,” *Nature*, vol. 526, no. 1, pp. S90–S91, 2015.
- [3] T. Li, W. Xu, L. Wang, Y. Ren and J. Xia, “An integrated artificial neural network-based precipitation revision model,” *KSII (Korean Society for Internet Information) Transactions on Internet and Information Systems*, vol. 15, no. 5, pp. 1690–1707, 2021.
- [4] B. K. Remesh, K. G. Preetha, S. Saritha and K. R. Rinil, “An energy efficient intelligent method for sensor node selection to improve the data reliability in internet of things networks,” *KSII (Korean Society for Internet Information) Transactions on Internet and Information Systems*, vol. 15, no. 9, pp. 3151–3168, 2021.
- [5] S. V. Prasanna, K. Balasubadra, K. Saravanan, V. S. Arjun and S. Malarkodi, “Multi label deep learning classification approach for false data injection attacks in smart grid,” *KSII (Korean Society for Internet Information) Transactions on Internet and Information Systems*, vol. 15, no. 6, pp. 2168–2187, 2021.
- [6] K. Xu, “Electrolytes and interphases in Li-Ion batteries and beyond,” *Chemical Reviews*, vol. 114, no. 23, pp. 11503–11618, 2014.
- [7] Z. Yu, D. G. Mackanic, Y. Cui and Z. Bao, “A dynamic, electrolyte-blocking, and single-ion-conductive network for stable lithium-metal anodes,” *Joule*, vol. 3, no. 11, pp. 2761–2776, 2019.
- [8] X. Xu, Z. Wen, X. Wu, X. Yang and Z. Gu, “Lithium ion-conducting glass-ceramics of  $Li_{1.5}Al_{0.5}Ge_{1.5}(PO_4)_{3-x}Li_2O$  ( $x=0.0-0.20$ ) with good electrical and electrochemical properties,” *Journal of the American Ceramic Society*, vol. 90, no. 9, pp. 2802–2806, 2007.
- [9] D. Lin, Y. Liu, Z. Liang, J. Xie and Y. Cui, “Layered reduced graphene oxide with nanoscale interlayer gaps as a stable host for lithium metal anodes,” *Nature Nanotechnology*, vol. 11, pp. 626–632, 2016.
- [10] A. Manthiram, X. Yu and S. Pocharski, “Lithium battery chemistries enabled by solid-state electrolytes,” *Nature Reviews Materials*, vol. 2, no. 16103, pp. 1–16, 2017.
- [11] P. G. Bruce and A. R. West, “The A-C conductivity of polycrystalline LISICON,  $Li_{2+2x}Zn_{1-x}GeO_4$ , and a model for intergranular constriction resistances patterns,” *Journal of the Electrochemical Society*, vol. 130, no. 3, pp. 662–663, 1983.

- [12] A. Emly, E. Kioupakis and A. Van der Ven, "Phase stability and transport mechanisms in antiperovskite  $\text{Li}_3\text{OCl}$  and  $\text{Li}_3\text{OBr}$  superionic conductors," *Chemistry of Materials*, vol. 25, no. 23, pp. 4663–4670, 2013.
- [13] X. Han, Y. Gong, K. K. Fu, E. D. Wachsman and L. Hu, "Negating interfacial impedance in garnet-based solid-state Li metal batteries," *Nature Materials*, vol. 16, pp. 572–579, 2017.
- [14] F. Mizuno, A. Hayashi, K. Tadanaga and M. Tatsumisago, "A large area flexible array sensors using screen printing technology," *Advanced Materials*, vol. 17, no. 7, pp. 918–921, 2005.
- [15] M. Matsuo, Y. Nakamori, S.-I. Orimo, H. Maekawa and H. Takamura, "Lithium superionic conduction in lithium borohydride accompanied by structural transition," *Applied Physics Letters*, vol. 91, no. 22, pp. 224103–224106, 2007.
- [16] W. Liu, S. W. Lee, D. Lin, A. D. Sendek and Y. Cui, "Enhancing ionic conductivity in composite polymer electrolytes with well-aligned ceramic nanowires," *Nature Energy*, vol. 2, no. 17035, pp. 1–7, 2017.
- [17] J. S. Thokchom and B. Kumar, "Composite effect in superionically conducting lithium aluminium germanium phosphate based glass-ceramic," *Journal of Power Sources*, vol. 185, no. 1, pp. 480–485, 2008.
- [18] M. Guin, S. Indris, M. Kaus, H. Ehrenberg and O. Guillon, "Stability of NASICON materials against water and  $\text{CO}_2$  uptake," *Solid State Ionics*, vol. 302, no. 1, pp. 102–106, 2017.
- [19] Z. Sun, L. Liu, Y. Lu, J. Zhao and H. An, "Preparation and ionic conduction of  $\text{Li}_{1.5}\text{Al}_{0.5}\text{Ge}_{1.5}(\text{PO}_4)_3$  solid electrolyte using inorganic germanium as precursor," *Journal of the European Ceramic Society*, vol. 39, no. 2, pp. 402–408, 2019.
- [20] P. Hartmann, T. Leichtweiss, M. R. Busche, P. Adelhelm and J. Janek, "Degradation of NASICON-type materials in contact with lithium metal: Formation of mixed conducting interphases (MCI) on solid electrolytes," *The Journal of Physical Chemistry C*, vol. 117, no. 41, pp. 21064–21074, 2013.
- [21] J. A. Lewis, F. J. Q. Cortes, M. G. Boebinger, M. Chi and M. T. McDowell, "Interphase morphology between a solid-state electrolyte and lithium controls cell failure," *ACS (American Chemical Society) Energy Letter*, vol. 4, no. 2, pp. 591–599, 2019.
- [22] Y. Liu, C. Li, B. Li, H. Song, P. He *et al.*, "Germanium thin film protected lithium aluminum germanium phosphate for solid-state Li batteries," *Advanced Energy Materials*, vol. 8, no. 16, pp. 1702374–1702379, 2018.
- [23] Z. Zhang, S. Chen, J. Yang, P. Cui and X. Xu, "Stable cycling of all-solid-state lithium battery with surface amorphized  $\text{Li}_{1.5}\text{Al}_{0.5}\text{Ge}_{1.5}(\text{PO}_4)_3$  electrolyte and lithium anode," *Electrochimica Acta*, vol. 297, no. 1, pp. 281–287, 2019.
- [24] S. K. Singh, H. Gupta, Y. L. Verma and R. K. Singh, "Improved electrochemical performance of EMIMFSI ionic liquid based gel polymer electrolyte with temperature for rechargeable lithium battery," *Energy*, vol. 150, no. 1, pp. 890–900, 2018.
- [25] D. R. MacFarlane, M. Forsyth, P. C. Howlett, S. Zhang and J. Zhang, "Ionic liquids and their solid-state analogues as materials for energy generation and storage," *Nature Reviews Materials*, vol. 1, no. 15005, pp. 1–10, 2016.
- [26] I. A. Shkrob, T. W. Marin, Y. Zhu and D. P. Abraham, "Why B is (fluorosulfonyl)imide is a magic anion for electrochemistry," *The Journal of Physical Chemistry C*, vol. 118, no. 34, pp. 19661–19671, 2014.
- [27] S. Xiong, K. Xie, E. Blomberg, P. Jacobsson and A. Matic, "Analysis of the solid electrolyte interphase formed with an ionic liquid electrolyte for lithium-sulfur batteries," *Journal of Power Sources*, vol. 252, no. 1, pp. 150–155, 2014.
- [28] Y. Lu, Z. Tu and L. A. Archer, "Stable lithium electrodeposition in liquid and nanoporous solid electrolytes," *Nature Materials*, vol. 13, no. 1, pp. 961–969, 2014.
- [29] P. Jankowski, N. Lindahl, J. Weidow, W. Wiczczonek and P. Johansson, "Impact of sulfur-containing additives on lithium-ion battery performance: From computational predictions to full-cell assessments," *ACS (American Chemical Society) Applied Energy Materials*, vol. 1, no. 6, pp. 2582–2591, 2018.
- [30] H. Yildirim, J. B. Haskins, C. W. Bauschlicher and J. W. Lawson, "Decomposition of ionic liquids at lithium interfaces. 1. Ab Initio molecular dynamics simulations," *The Journal of Physical Chemistry C*, vol. 121, no. 51, pp. 28214–28234, 2017.

- [31] A. J. Louli, L. D. Ellis and J. R. Dahn, "Operando pressure measurements reveal solid electrolyte interphase growth to rank li-ion cell performance," *Joule*, vol. 3, no. 3, pp. 745–761, 2019.
- [32] J. Nordström, L. Aguilera and A. Matic, "Effect of lithium salt on the stability of dispersions of fumed silica in the ionic liquid BMImBF<sub>4</sub>," *Langmuir*, vol. 28, no. 9, pp. 4080–4085, 2012.
- [33] B. Commarieu, A. Paoella, J.-C. Daigle and K. Zaghbi, "Toward high lithium conduction in solid polymer and polymer-ceramic batteries," *Current Opinion in Electrochemistry*, vol. 9, no. 1, pp. 56–63, 2018.
- [34] F. Sagane, T. Abe and Z. Ogumi, "Electrochemical analysis of lithium-ion transfer reaction through the interface between ceramic electrolyte and ionic liquids," *Journal of The Electrochemical Society*, vol. 159, no. 11, pp. 1766–1770, 2012.
- [35] M. R. Busche, T. Drossel, T. Leichtweiss, P. Adelhelm and J. Janek, "Dynamic formation of a solid-liquid electrolyte interphase and its consequences for hybrid-battery concepts," *Nature Chemistry*, vol. 8, no. 1, pp. 426–434, 2016.
- [36] X. He, P. W. Fuerschbach and T. DebRoy, "Heat transfer and fluid flow during laser spot welding of 304 stainless steel," *Journal of Physics D: Applied Physics*, vol. 36, no. 12, pp. 1388–1392, 2003.
- [37] A. C. Ferrari, "Raman spectroscopy of graphene and graphite: Disorder, electron-phonon coupling, doping and nonadiabatic effects," *Solid State Communications*, vol. 143, no. 1, pp. 47–57, 2007.
- [38] Q. Zhao, X. T. Liu, S. Stalin, K. Khan and L. A. Archer, "Solid-state polymer electrolytes with in-built fast interfacial transport for secondary lithium batteries," *Nature Energy*, vol. 4, no. 1, pp. 365–373, 2019.